Available online at www.sciencedirect.com

ScienceDirect

IFAC PapersOnline CONFERENCE PAPER ARCHIVE

IFAC PapersOnLine 55-16 (2022) 142–147

Health-Constrained Explicit Model Predictive Control Based on Deep-Neural Networks Applied to Real-Time Charging of Batteries

Ahmed Shokry*[1], Eric Moulines*[2]

**Center for Applied Mathematics, Ecole Polytechnique, Route de Saclay, 91120 Palaiseau, France.*
[1]ahmed.shokry@polytechnique.edu

[2]eric.moulines@polytechnique.edu

Abstract: The application of Model Predictive Control (MPC) for optimal real-time battery charging is attracting growing interest due to its advantages over empirical charging protocols. However, the high complexity and nonlinearity of physics-based models of batteries can hinder MPC applications due to the large computational resources required online. To overcome this challenge, this paper proposes a machine learning (ML) based explicit MPC method for battery charging subjected to health constraints. The method uses deep artificial neural networks (DANNs) to construct offline control laws that describe the optimal charging current as a function of the state of the battery. These DANN-based control laws are developed using data generated by solving the MPC problem using the physics-based model of the battery and considering different expectations for the initial state of the battery. These control laws can then be used online to control the charging process by calculating the optimal closed-loop current via simple and inexpensive predictions. The method is applied to a case study of battery charging based on MPC, and the results prove the capabilities of the DANN-based control laws in terms of i) very high prediction accuracy of the closed-loop profiles of the charging current, ii) good ability to learn the constraints imposed on the MPC problem from the data, and iii) significant reduction in the required computation time compared to traditional MPC.

Keywords: Batteries; Charging; Battery Health; Constrained Model Predictive Control; Explicit Control; Deep Artificial Neural Networks.

1. INTRODUCTION

Rechargeable batteries are the main power storage and supply units in a variety of sectors, such as smart grids and transportation. In general, batteries are complex components with complicated electrochemical reactions, thermoelectric effects, and degradation phenomena (Gao et al., 2020). In addition, batteries operate under uncertain and dynamic conditions in terms of operational policies and environmental practices. These challenges make batteries critical to the functionality and safety of the systems in which they operate. As a result, the development of battery management systems (BMS) is of great importance to ensure optimal operation of the battery, ultimately extending its lifetime (Rosewater et al., 2019). One of the main functions of a BMS is to control battery charging to achieve the best performance in terms of minimizing charging time while maintaining the health of the battery in long-term operation by meeting important safety and health constraints, such as extreme overvoltage (Rosewater et al., 2019). Most industrial BMSs use standard charging protocols that guarantee a reasonable trade-off between charging time and battery health (Gao et al., 2020). Constant current-constant voltage is the most common charging protocol, in which the battery is charged with a predefined constant current until its terminal voltage rises to a predefined threshold. Then the battery starts to be charged at a constant voltage, resulting in an exponential decrease of the charging current (Tian et al., 2021). These protocols are experimentally defined based on the nominal characteristics of the battery, so they ignore the varying online operating conditions and lack of knowledge about the electrical or thermal dynamics of the battery (Goldar et al., 2020). To overcome these limitations, advanced BMSs currently treat the battery charging process as a MPC problem, where a controller steers the system to a set-point represented by the required state of charge (SOC) (Rosewater et al., 2019). This framework not only ensures fast charging, but more importantly, enables i) the use of available knowledge about battery dynamics represented by its accurate physics-based models, and ii) the flexible imposition of necessary safety and health requirements (i.e., constraints) on the charging process. Many works have studied the optimal charging of batteries by applying MPC technology. The main differences among these studies are mainly the type of physics-based model involved in the MPC problem, e.g., equivalent circuit models and equivalent hydraulic models. A detailed review of battery charging MPC, focusing on the different models considered, can be found in (Rosewater et al., 2019). Despite these increasing advances in the application of MPC to battery charging, one major challenge is typically reported, which is that most hardware components of industrial BMSs are unable to support the computational cost required to solve an open-loop optimal control problem online at each sampling period (SP) (Tian et al., 2021). This represents an obstacle to the commercialization of this efficient battery charging technology.

10.1016/j.ifacol.2022.09.014

In other fields, to tackle this problem, explicit MPC (E-MPC) methods have been proposed, in which explicit control laws are developed offline to approximate the optimal values of the control variables to be applied in the future SP as functions of the state variables at the current SP. These control laws are then used online to compute the optimal values of the control variables via simple function evaluations, saving enormous computational costs required for dynamic optimization in MPC (Pistikopoulos et al., 2011). Two main approaches have been considered for the development of control laws, namely multiparametric MPC (MP-MPC) and ML-based explicit MPC (ML-E-MPC). The MP-MPC provides very simple mathematical control laws in the form of piecewise affine functions that describe the relationship between the optimal control and the state variables of the system (Pistikopoulos et al., 2011). However, the application of MP-MPC is limited to small systems for which linear, discrete-time state-space models are available. This complicates its direct application in situations where complex and highly nonlinear models of the system must be considered, such as battery models. The second approach, ML-E-MPC, relies on training ML models to capture the mapping between control and state variables that represent data-driven control laws (Karg and Lucia, 2020; Kis et al., 2021).

To our best knowledge, only one work (Tian et al., 2021) has proposed the MP-MPC for low-cost battery charging control, while the ML-E-MPC approach has not yet exploited. Also, although the capabilities of ML-E-MPC have been demonstrated in the literature in several areas (Shokry et al., 2016; Kis et al., 2021), there are some limitations: i) it has been applied mainly considering linear dynamic models, and ii) its ability to handle constraints imposed on MPC problems has not been sufficiently studied, e.g., it has been applied only to MPC cases involving bound constraints on the control and/or state variables. Therefore, this work presents an efficient ML-E-MPC method for health-constrained charging of batteries. The method aims at solving general MPC problems where a nonlinear dynamic model of the system must be considered along with various constraints, such as bounds on control and state variables and linear functions of states (e.g., health constraints). The method develops offline control laws using DANNs which approximate the mapping between the future values of the control variables and the current values of the state variables. The data used to build these DANNs are obtained by solving the MPC problem multiple times corresponding to different values of the initial state variables, which are carefully selected by Design Of Computer Experiment (DOCE) techniques. Then, the developed DANNs-based control laws can be used in a closed loop to control the charging process in real time. The method is applied to a case study adopted from the literature involving the health-constrained MPC of battery charging process.

2. PROBLEM STATEMENT

MPC relies on an accurate dynamic model, $\boldsymbol{F}$, of the real system (3), which describes the relations among state $x \in R^m$ and control variables $u \in R^v$, and on a cost function J (1) that must be minimized considering a number of L constraints $g_l, l = 1, \dots, L$ (4). The total period with which the system is required to reach its set-point, $\check{r} \in R^{\check{m}}$, $\check{m} \leq m$, is discretized into equal number of N^{fnl} SP and, then, at each SP $k = 1, \dots, N^{fnl}$ the following steps are implemented: i) the model, $\boldsymbol{F}$, is updated by the real measurements of the state/output variables collected from the system by the physical sensors, which represent the Initial Conditions (IC) of the model at this SP (2), and then ii) a dynamic optimization problem is solved based on $\boldsymbol{F}$ to find the optimal profile of the control input variables $[u^*_{t+1}, \dots, u^*_{t+N_p}]$ over a prediction horizon N_p. Then, only the values of the optimal control profile corresponding to the first SP, u^*_{t+1}, are implemented in the real system, and at its end, the state/output variables are measured and their values are used as IC to setup the next open-loop optimal control problem, and so on (Pistikopoulos et al., 2011). The final solution of a MPC problem is defined by the optimal close-loop trajectory of control $[u^*_1, \dots, u^*_k, , \dots, u^*_{N^{fnl}}]$ and the associated trajectory of state variables $[x_0, \dots, x_k, \dots, x_{N^{fnl}-1}]$.

$$\min_{u_{t+1},\dots,u_{t+N_p}} J = x'_{t+N_p} P\, x_{t+N_p} + \sum_{k=1}^{N_p-1} [(x_{t+k} - \check{r})'\, Q\, (x_{t+k} - \check{r}) + \Delta u'_{t+k}\, \mathcal{R}\, \Delta u_{t+k}] \quad (1)$$

$$x_t = IC, \qquad k = 0 \quad (2)$$

$$x_{t+k+1} = \boldsymbol{F}(x_{t+k}, u_{t+k}),\ x \in R^m, u \in R^v \quad (3)$$

$$g_l(x_{t+k}, u_{t+k}) \leq 0\,, \quad l = 1,2, \dots L,\ k = 1, \dots, N_c \quad (4)$$

$$x_{min} \leq x_{t+k} \leq x_{max} \quad (5)$$

$$u_{min} \leq u_{t+k} \leq u_{max} \quad (6)$$

$$\Delta u_{t+k} = u_{t+k} - u_{t+k-1},\ k = 1,2, \dots, N_p \quad (7)$$

Notice that the MPC problem involves time-discretization parameters, such as the prediction horizon N_p, the control horizon N_u and the constraints horizon N_c, besides the objective weighting parameters such as P, Q and $\mathcal{R}$, which are matrices of sizes $\check{m} \times \check{m}$, $\check{m} \times \check{m}$ and $v \times v$, respectively. In general, the choice of the values of these parameters is case dependent decision (Pistikopoulos et al., 2011). This work considers cases where the available dynamic model, $\boldsymbol{F}$, is complex and highly nonlinear, which are common features of the most available models of batteries. These challenges can easily obstacle both the efficient application of the MPC scheme and, also, the mathematical E-MPC methods.

3. METHOD

3.1 Step 1: Sampling of the Initial State Values

The first step is to generate offline training and testing datasets to be used for the control laws development. The training dataset should contain information about the behavior of the controller when departing from all the possible subspaces of the state variables (Garud et al., 2017). This increases the likelihood that the resulting ML-based control laws will exhibit efficient and robust performance. To this end, DOCE techniques are used to sample over the space of the state variables $x_{min} \leq x_{t+k} \leq x_{max}$ to select a proper set of n^{tr}

combinations of the ICs $[x_{0,i}],\ i = 1, \dots, n^{tr},\ x \in \mathrm{R}^m$. We use a hybrid DOCE method that combines the use of Hammersley sequences and factorial designs, as it is able to generate sampling plans with high uniformity at very low computational cost. The factorial design collects samples at the boundaries and vertices of the input space, while the Hammersley procedure selects uniform samples over most of the input space (Shokry et al., 2016).

3.2 Step 2: MPC Solution for Data Generation

In this step, the constrained MPC problem ((1):(7)) is solved n^{tr} times, but only over a finite horizon $N^{trn} \leq N^{fnl}$, where, in each time, one combination of the ICs set, $x_{0,i}$, is considered in (2). This allows to obtain the optimal trajectories of the close-loop control $[u^*_{1,i}, \dots, u^*_{N^{trn},i}]$ and the associated trajectories of the state variables $[x_{0,i}, \dots, x_{N^{trn}-1,i}],\ i = 1, \dots, n^{tr}$. Then, the n^{tr} pairs of state-control trajectories are unfolded into a set of input-output patterns in the form of $\left[x_{t,i},\ u^*_{t+1,i}\right], i = 1, \dots, n^{tr} \times N^{trn}$. A test dataset is generated in the same way, as described in Sections 3.1 and 3.2, but this time, the MPC problem is solved over the entire horizon N^{fnl} to obtain n^{ts} pairs of optimal state-control trajectories corresponding to different n^{ts} ICs, i.e., $[x^{ts}_{0,i}, \dots, x^{ts}_{N^{fnl}-1,i}]$-$[u^{*ts}_{1,i}, \dots, u^{*ts}_{N^{fnl},i}],\ i = 1, \dots, n^{ts}$. These test control-state trajectories are also unfolded into input-output dataset $[x^{ts}_{t,i}, u^{*ts}_{t+1,i}], i = 1, \dots, n^{ts} \times N^{fnl}$. The unfolded test data set is used to assess the open-loop accuracy of the control laws, while the n^{ts} pairs of state-control trajectories are used to assess their closed-loop accuracy.

Various methods can be used to solve the dynamic optimization problem embedded in the MPC scheme, such as Control Vector Parametrization (CVP), direct multiple shooting, and collocation methods (Biegler, 2007). This work uses the CVP method due to its implementation simplicity, in which the control variables are discretized in the form of piecewise low order polynomials, and then a non-linear programming optimization problem is carried out in the space of the discretized control variables (Shokry & Espuña, 2014). In this work, the Matlab "*fmincon*" solver has been used, based on a sequential quadratic programming algorithm, for constrained nonlinear optimization.

3.3 Step3: Control Laws Development based on DANNs

The training dataset $\left[x_{t,i}\right] - \left[u^*_{t+1,i},\right], i = 1, \dots, n^{tr} \times N^{trn}$, $x \in R^m, u \in R^v$, is used to develop a number of v ML-based control laws $\hat{u}^*_{i,t+1} = \mathcal{F}_{DANNi}(x_t),\ i = 1, \dots, v$, where, $\mathcal{F}_{DANNi}$ are feedforward DANNs. Each of these laws approximates the optimal values of a control variable at the next SP as a function of the values of the state variables at the current SP. In this work, deep learning models are used due to their powerful capabilities to approximate the behavior of complex systems. These capabilities derive from their deep architecture, which consists of multiple nonlinear data processing stages that enable better learning of the hidden hierarchical representation of latent information in the data. A feedforward DANN consists of multiple data processing units, called neurons, arranged in a structure with a certain number of layers. The neurons are interconnected, with the importance of each connection calibrated by a weight value. Training an ANN involves an optimization problem in which the optimal values of the weights and biases are determined by minimizing a cost function related to the errors between the predicted outputs and their target values. In this work, the Matlab functions *"feedforwardnet"* and "*trainbr*" were used to build and train the ANNs, respectively. The selection of the number of hidden layers, their respective sizes, and the training algorithm is done by a cut-and-try procedure that balances the prediction accuracy and the simplicity of the structure.

After training the DANN-based control laws, their open-loop response performance is evaluated using the unfolded test set $[x^{ts}_{t,i}, u^{*ts}_{t+1,i}], i = 1, \dots, n^{ts} \times N^{fnl}$ generated in Section 3.2, and an accuracy measure, such as the Normalized Root Mean Square Error (NRMSE) (8), can be calculated for each of the v control laws, where u^{*ts}_{max} and u^{*ts}_{min} are the maximum and minimum values of the control variables in the test set.

$$NRMSE = 100 \times \frac{\sqrt{\frac{1}{n^{ts} \times N^{fnl}} \sum_{i=1}^{n^{ts} \times N^{fnl}} (u^{*ts}_{t+1,i} - \hat{u}^{*ts}_{t+1,i})^2}}{(u^{*ts}_{max} - u^{*ts}_{min})} \quad (8)$$

3.4 Step 4: Online (closed-loop) Deployment

In the final step, the DANN-based control laws are embedded in a closed-loop to predict the entire control trajectory starting from arbitrary IC of the state variables. Hence, the closed-loop accuracy metrics of the control laws are evaluated using the n^{ts} pairs of control-state trajectories generated in Section 3.2, as follows:

i) by comparing the control trajectories predicted by the DANNs, $[\hat{u}^{*ts}_{1,i}, \hat{u}^{*ts}_{2,i}, \dots, \hat{u}^{*ts}_{N^{fnl},i}]$, with their exact optimal values, $[u^{*ts}_{1,i}, u^{*ts}_{2,i}, \dots, u^{*ts}_{N^{fnl},i}]$, a closed-loop NRMSE can be calculated for each control trajectory and then averaged over the n^{ts} trajectories.

ii) by comparing the system state resulting from applying the predicted control trajectories, $[x^{ts}_{0,i}, \tilde{x}^{ts}_{1,i}, \dots, \tilde{x}^{ts}_{N^{fnl}-1,i}]$, with their exact optimal values, $[x^{ts}_{0,i}, x^{ts}_{1,i}, \dots, x^{ts}_{N^{fnl}-1,i}]$, a closed-loop NRMSE can be computed for each state trajectory and then averaged of the n^{ts} trajectories.

iii) by comparing the predicted n^{ts} control and their resulting states trajectories to the limits of the constraints ((4), (5) and (6)), constraint violation metrics can be calculated, which quantifies the ability of the DANN based control laws to learn the constraints imposed on the MPC problem.

4. APPLICATION

This application considers a nonlinear double-capacitor (NDC) model (Tian et al., 2021), which can be seen as two electric circuits: the first one represents an electrode storing electric charge, which is modeled as two capacitor-resistor $(C_b - R_b, C_s - R_s)$ connected in parallel. The $R_s - C_s$ part represents the electrode surface exposed to the electrode-

electrolyte interface and mimics the high-frequency part of the charging/discharging response. The $R_b - C_b$ part acts as the electrode's inner bulk and emulates the low-frequency response. The second circuit is composed by *i*) a voltage source $U = f_1(V_s)$ (see (13)), where V_s is the voltage across C_s and *ii*) a resistance R_0 representing the electrolyte resistance and is modeled as a function of the SOC, i.e., $R_0 = f_2(SOC)$ (see (14)). Hence, the NDC dynamics can be described as:

$$\begin{bmatrix} \dot{V}_b(t) \\ \dot{V}_s(t) \end{bmatrix} = A \begin{bmatrix} V_b(t) \\ V_s(t) \end{bmatrix} + B\, I(t) \tag{9}$$

$$SOC(t) = [C_b V_b(t) + C_s V_s(t)]\,/C_b + C_s \tag{10}$$

$$V_{tr}(t) = U(t) + R_0(t)\, I(t) \tag{11}$$

$$A = \begin{bmatrix} -1/C_b\,(R_b + R_s) & 1/C_b\,(R_b + R_s) \\ 1/C_s\,(R_b + R_s) & -1/C_s\,(R_b + R_s) \end{bmatrix},\ B = \begin{bmatrix} R_s/C_b\,(R_b + R_s) \\ R_b/C_s\,(R_b + R_s) \end{bmatrix} \tag{12}$$

$$U(t) = \alpha_0 + \alpha_1 V_s(t) + \alpha_2 V_s(t)^2 + \alpha_3 V_s(t)^3 + \alpha_4 V_s(t)^4 + \alpha_5\, V_s(t)^5 \tag{13}$$

$$R_0(t) = \beta_0 + \beta_1\, exp\left(-\beta_3\left(1 - SOC(t)\right)\right) \tag{14}$$

where $V_b(t)$ is the voltage across C_b, $I(t)$ is the applied current and $V_{tr}(t)$ is the battery terminal voltage. The values of the parameters $\{C_b, C_s, R_b, R_s, \beta_0, \beta_1, \beta_3, \alpha_1, \alpha_2, \alpha_3, \alpha_4, \alpha_5\}$ have been experimentally identified in (Tian et al., 2021). From (9):(14), it can be noted that $V_b(t)$ and $V_s(t)$ determine the entire state of the system. The variability of $V_s(t)$ is set between the bounds [0,1], being that at the maximum capacity, $SOC(t) = 100\%$, $V_b(t) = V_s(t) = 1$, while at the minimum capacity, $SOC(t) = 0\,\%$, $V_b(t) = V_s(t) = 0$.

In this case, a MPC problem ((15):(20)) is addressed to charge the battery, starting from an initial charge $SOC_0 = 20\%$ and reaching to a set-point $\check{r}$= 90% of charge (16) within a maximum of N^{fnl}=150 SP each includes 60 s. Safety requirements imply bounds on the applied current I_{t+k} (17) and an upper bound on the terminal voltage $V_{tr,t+k}$ (18). Finally, a health constraint associated to charge migration from the surface to the bulk of the electrode is also considered (19).

The proposed method is applied following the steps described in Section 3. The first step is to sample over the estimated domain of the state variables [$V_{s,min}$= 0.0: $V_{s,max}$= 0.9, $V_{b,min}$= 0.0: $V_{b,max}$=0.9] using the hybrid DOCE technique to generate the ICs matrix $[V_{s0,i}, V_{b0,i}]_{i=1:400}$. Then the MPC problem is solved 400 times over a horizon of $N^{trn} = 5$ SP to obtain the optimal trajectories of the closed-loop control $\left[I^*_{1,i}, \dots, I^*_{5,i}\right]_{i=1:400}$ and the associated states $\left[V_{s0,i}, \dots, V_{s4,i}\right]_{i=1:400}$, $\left[V_{b0,i}, \dots, V_{b4,i}\right]_{i=1:400}$, which are then unfolded into the input-output training matrix $\left[V_{s\,t,i}, V_{b\,t,i}, I^*_{t+1,i}\right]_{i=1:2000}$. Using this input-output dataset, a DANN-based control law, $\hat{I}^*_{t+1} = \mathcal{F}^{NDC}_{DANN}(V_{s,t}, V_{b,t})$, is trained. The network structure is set as 3 hidden layers with 7, 5 and 3 neurons, while a Bayesian regularization backpropagation algorithm is used for training, which minimizes a loss function containing the sum of the network prediction errors and also the sum of its weights to obtain good regularization properties.

A test dataset is generated that includes a number of $n^{ts} = 30$ optimal closed-loop control profiles , $\left[I^{*ts}_{1,i}, \dots, I^{*ts}_{150,i}\right]_{i=1:30}$, and the associated state, $\left[V^{ts}_{s\,0,i}, \dots, V^{ts}_{s\,149,i}\right]_{i=1:30}$ and $\left[V^{ts}_{b\,0,i}, \dots, V^{ts}_{b\,149,i}\right]_{i=1:30}$. The unfolded form of the test set, $\left[V^{ts}_{b\,t,i}, V^{ts}_{s\,t,i}, I^{*ts}_{t+1,i}\right]_{i=1:4500}$, is used to evaluate the open-loop/offline performance of the control law, while the entire trajectories are used to evaluate its closed-loop/online performance. The testing results, summarized in Table 1 and Table 2, emphasize the promising performance of the DANN-based control law in terms of i) the high open-loop accuracy (NRMSE of 0.9 %) ii) high closed-loop accuracy of the 30 predicted charging current trajectories (NRMSE of 0.38 %), iii) high closed-loop accuracy of the state variables resulted from the application of the predicted charging trajectories (NRMSEs less than 1.0 %), and iv) low online computational overhead required to predict the 30 closed-loop control trajectories (84.6 s) compared to that of mathematical MPC (2629.8 s). Also, Figure 1 evidences the high accuracy of the developed DANN-based control law.

$$\min_{I_{t+1},\dots,I_{t+N_p}} J = \sum_{k=1}^{N_p - 1} [(SOC_{t+k} - \check{r})'\, Q\, (SOC_{t+k} - \check{r}) + \Delta I'_{t+k}\, \mathcal{R}\, \Delta I_{t+k}] \tag{15}$$

S.T.:

$$SOC_0 = 20\%, \qquad \check{r} = 90\% \tag{16}$$

$$0 \le I_{t+k} \le 3\ A, \qquad k = 1, \dots, N_p \tag{17}$$

$$V_{tr,t+k} \le 4.2\ \ V, \qquad k = 1, \dots, N_c \tag{18}$$

$$V_{s,t+k} - V_{b,t+k} \le -0.04\, SOC_{t+k} + 0.08,\ k = 1, \dots, N_c \tag{19}$$

$$\dot{V_{b,t}}, \dot{V_{s,t}}, SOC_t, V_{tr,t} = \boldsymbol{F}(\dots), \quad \boldsymbol{F} \text{ is the NDC model} \tag{20}$$

$$N_p = 10,\ N_u = 2,\ N_c = 1, Q = 1,\ R = 0.1$$

Table 1. Offline computational cost and open-loop accuracy.

*Offline CPU time (s)**			*Open-loop control accuracy (NRMSE (%))*
Data generation		*DANN fitting*	
Training	*Testing*		
1834.9	2629.8	10.2	0.9

**Intel core (TM) i7-8565U CPU@ 18 GHz, 12 GB RAM.*

Table 2. Online computational cost and closed-loop accuracy.

Closed-loop control accuracy (NRMSE (%))	*Resulting closed-loop states accuracy (NRMSE (%))*				*Online CPU time (s)**	*Saved time %*
	V_b	V_s	V_{tr}	SOC		
0.38	0.52	0.50	0.79	0.54	84.6	96.8

Table 3 shows the very low average and maximum constraint violations realized by the predicted closed-loop control trajectories and resulting states, which confirm the high capabilities of the DANN-based control law to learn the constraints ((17), (18) and (19)) of the MPC problem from data, without any prior knowledge about its mathematical formulation. Figure 2-(a) shows the 30 predicted closed-loop

trajectories of charging current versus the resulting terminal voltage (colored crosses and colored dashed lines) compared to their exact values (grey hollow circles and grey solid lines). Note that each predicted trajectory is denoted by a different color, starts from a different IC (represented by a filled colored circle), and ends at the steady state of the system (represented by a yellow star). Also, in Figure 2, the horizontal and vertical solid black lines represent the current and terminal voltage constraints, respectively. The figure shows the high accuracy of the DANN-based control law and its good ability to learn the constraints for the current and the terminal voltage.

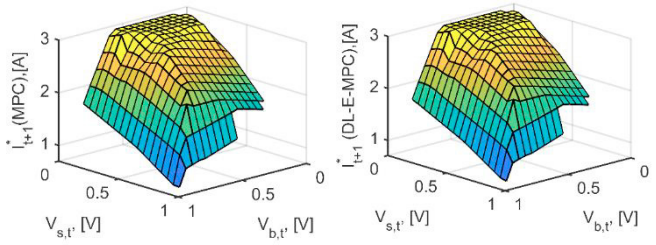

Figure 1. Exact (left) vs. DANN-based control law (right).

Table 3. Average and maximum constraint violations.

	Constraint 1		*Constraint 2*	*Constraint 3*
	$I_t \leq 3$	$I_t \geq 0$	$V_{tr,t} \leq 4.2$	$V_{s,t} - V_{b,t} \leq -0.04\,SOC_t + 0.08$
Average	0	0	4.50×10^{-4}	4.80×10^{-5}
Maximum	0	0	9.64×10^{-4}	2.43×10^{-4}

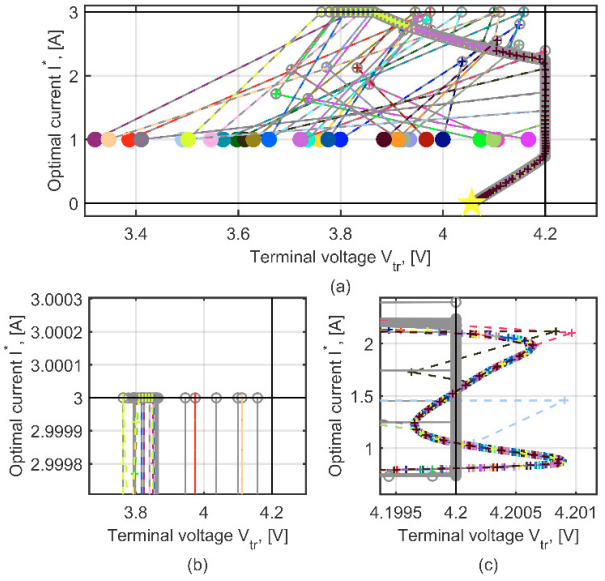

Figure 2. Thirty predicted vs. exact closed-loop trajectories of current and the resulting terminal voltage (a), along with zoomed-in details (b, c). Colored filled circle are ICs; colored crosses and colored dashed lines are the predicted behaviors; grey hollow circles and grey solid lines are the exact behaviors; yellow star is the steady-state.

Figure 3 illustrates the good ability of the DANN-based control law to learn the health constraint by showing the 30 predicted trajectories of current versus the health constraint (19), represented by a solid black line. Since the IC were randomly selected from the range of state variables, some of them are not feasible with respect to the health constraint, so they were excluded from the trajectories.

Figure 4 shows the time-evolution of three predicted closed-loop current trajectories (dashed lines in Figure 4-(e)) and the resulting state (dashed lines in Figure 4-(a,b,c,d)) compared to their exact values (solid lines). The three scenarios correspond to three different ICs. The figure again highlights the high accuracy of the predicted current trajectories and their ability to satisfy the terminal voltage and current constraints represented by the dashed black lines in Figure 4-(c, e). Figure 5 shows how the predicted control trajectories are able to precisely satisfy the health constraint in the three scenarios.

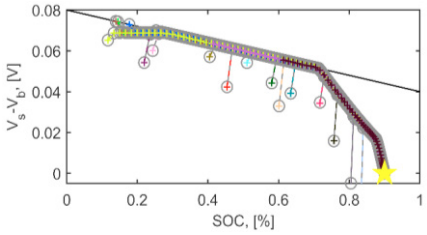

Figure 3. Predicted and exact closed-loop trajectories of current vs. the health constraint (solid black line), excluding the ICs.

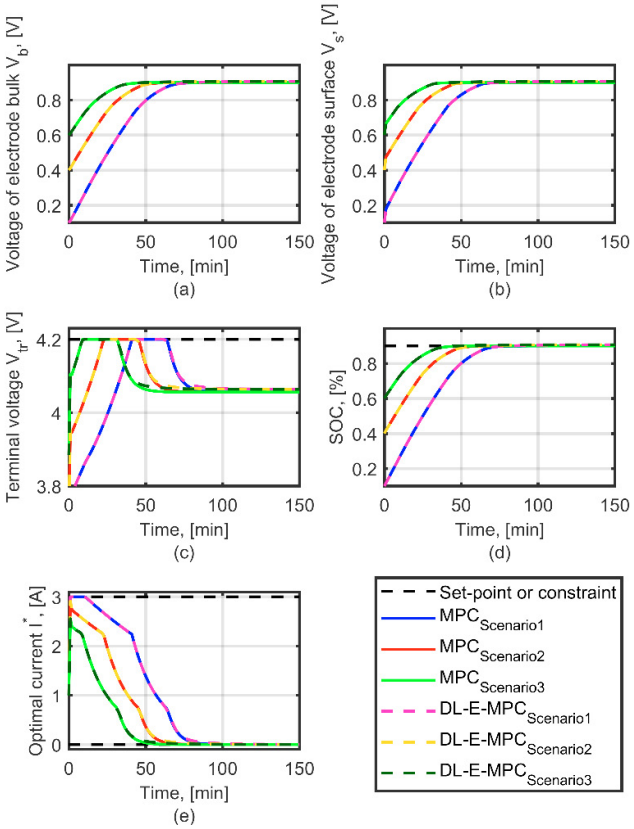

Figure 4. Closed-loop profiles of charging current predicted by the DANN-based control law and the resulting states (magenta, yellow and dark-green dashed lines) compared to their exact values (blue, red and green solid lines), considering three different ICs.

5. CONCLUSIONS

The complexity of most physics-based models of batteries can hinder the exploitation of the promising capabilities of MPC technologies for optimal charging, as it can lead to a large computational overhead required to repeatedly solve an open-loop optimal control problem at each SP. To overcome this challenge, this paper proposes a ML-E-MPC method for real-time optimal charging of batteries considering health constraints. The method was applied to a case study taken from the literature, which shows promising capabilities, including:

i) provision of DANN-based control laws capable of predicting charging current control profiles with high prediction accuracy (less than 1% NRMSE) and satisfying safety and health constraints for the charging process.

ii) robustness of the DANN-based control laws in terms of their ability to predict the accurate closed-loop charging current starting from arbitrary initial battery states.

iii) significant reduction in computation time compared to the mathematical solution of the MPC problem (96.8% time saving). This plays a key role in the commercialization of the optimal real-time charging technology through MPC, since the computational capabilities of most BMSs cannot afford the effort required to solve a MPC problem.

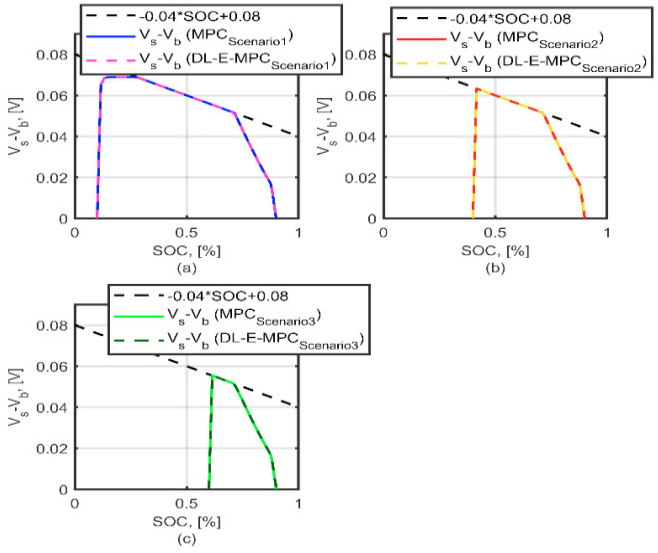

Figure 5. Predicted and exact closed-loop profiles of currents vs. the health constraint considering three different ICs.

Although the extensive numerical tests of the developed control law show very good closed-loop performance, it lacks a formal guarantee of closed-loop feasibility and stability, which is still an open question for most ML-based control methods in the literature (Karg and Lucia, 2020). Only a few recent works have developed certified guarantees for ML-based control laws through a posterior analysis of the safe/achievable ranges of the output of the trained control law, but most of them have been demonstrated using linear model predictive control cases (Karg and Lucia, 2020; Kumar et al., 2021). Future research will address improving the capabilities of the method in two main aspects: providing a formal feasibility and stability guarantee for the ML-based charging control laws, and considering unknown disturbances so as to develop robust charging control laws.

Acknowledgement: The authors acknowledge the support received from the *AI and predictive maintenance* chair of the Centre for Applied Mathematics- Ecole Polytechnique and Europorte.

REFERENCES

Biegler, L. T. (2007). An overview of simultaneous strategies for dynamic optimization. Chemical Engineering and Processing: Process Intensification, 46, 1043–1053.

Gao, S., Zhang, S., Guo, B., Zhu, C., Wiedemann, J., Wang, L., & Cao, J. (2020). Health-Aware Multiobjective Optimal Charging Strategy With Coupled Electrochemical-Thermal-Aging Model for Lithium-Ion Battery. IEEE Trans. Ind. Inform., 16, 3417-3429

Garud, S. S., Karimi, I. A., & Kraft, M. (2017). Design of computer experiments: A review. Comput. Chem. Eng., 106, 71–95.

Goldar, A., Romagnoli, R., Couto, L. D., Romero, A., Kinnaert, M., & Garone, E. (2020). MPC strategies based on the equivalent hydraulic model for the fast charge of commercial Li-ion batteries. Comput. Chem. Eng., 141, 107010.

Karg B., Lucia S. (2020). Stability and feasibility of neural network-based controllers via output range analysis. 59th IEEE Conference on Decision and Control, Korea.

Kis, K., Klauco, M., & Kvasnica, M. (2021). Explicit MPC in the form of Sparse Neural Networks. The 23rd International Conference on Process Control,163–168.

Kumar, P., Rawlings J., Wright, S. (2021). Industrial, large-scale model predictive control with structured neural networks. Comput. Chem. Eng., 150, 107291.

Pistikopoulos, E.N., Georgiadis, M. C., & Dua, V. (2011). Multi-Parametric Model-Based Control, Volume 2: Theory and Applications. In Wiley-VCH Verlag.

Rosewater, D. M., Copp, D. A., Nguyen, T. A., Byrne, R. H., & Santoso, S. (2019). Battery Energy Storage Models for Optimal Control. IEEE Access, 7, 178357–178391.

Shokry, A., Dombayci, C., & Espuña, A. (2016). Multiparametric Metamodels for Model Predictive Control of Chemical Processes. Computer Aided Chemical Engineering, 38(2), 937–942.

Shokry, A., & Espuña, A. (2014). Sequential Dynamic Optimization of Complex Nonlinear Processes based on Kriging Surrogate Models. Procedia Technology, 15, 376–387.

Tian, N., Fang, H., & Wang, Y. (2021). Real-Time Optimal Lithium-Ion Battery Charging Based on Explicit Model Predictive Control. IEEE Trans. Ind. Inform., 17, 1318–1330.